Original Research Article
Non-tipping Rod in Quiescent Water Based on Static Moment Equilibrium

ABSTRACT

In mechanics and engineering applications, the study of rigid bodies stability holds significant importance. The method of static moment equilibrium is a critical tool for analyzing the stability of rigid bodies. In this paper, a simple and practical non-tipping rod device is constructed, which can maintain balance in quiescent water without being overturned by an external wind force. The functional relationship between the inclination angle of the rod and the wind force was obtained through theoretical analysis, and the theoretical model was modified by the experimental data. The device is capable of detecting wind force up to 4.11±0.04 N (P=0.95) and can withstand at least the wind of near gale. This intuitive experimental device has potential applications in physics teaching and in the fields of wind detection engineering.

Keywords: Moment equilibrium; Gravitational torque; Three-axis sensor; Static stability

1. INTRODUCTION

Stability is a common phenomenon in nature, for example, a small ball would maintain stability at the center of a bowl in the absence of external forces, and a tumbler toy would remain upright when placed on a horizontal table [1-2].The investigation of the factors contributing to the stability of these objects has significantly advanced the progress and utilization of mechanics (e.g., [3-4]). The equilibrium characteristics of a mechanical system can be analyzed based on the principle of minimum potential energy [5-6].

The non-tipping rod is a classical system equilibrium problem that has attracted the attention of numerous researchers [7-8], and references therein. The equilibrium characteristics of the device can be briefly analyzed by using the knowledge of static moment equilibrium of rigid body mechanics (e.g., [9-10]). This type of research may possess practical application value in areas such as bioengineering [11], textile engineering [12], ocean engineering design [13-14], and so on. Simultaneously, by investigating this issue, we can further enhance our comprehension of the mechanical equilibrium problem, which holds certain reference value in physics teaching.

In this paper, a non-tipping rod device is designed, which can be capable of maintaining balance and stability in quiescent water under horizontal wind force. The device enables real-time monitoring of inclination angle through a wireless three-axis sensor in the rod. The buoyancy center can be adjusted via rod immersion ratio in water. The gravitational torque, buoyant torque, water plane restoring torque and wind force torque can be discussed through the analysis of rigid body model. Finally, a quantitative functional relationship between wind force and inclination angle is established, which is further modified and verified through experiments.

2. METHODOLOGY AND EXPERIMENTAL DETAILS

2.1 Experimental Apparatus

Experimental instruments: Bombo STEAM programming robot ET841, water, large sink, hollow plastic rod, 3-axis wireless inclinometer sensor, NaCl crystals, vernier caliper, glue gun, glue, high strength thin wire, rubber band, sealing ring, sealing cover, raw material belt, high precision electronic balance, anemometer, spring dynamometer, blower.

2.2 Static Moment Equilibrium Fundamentals

Figure 1 shows the schematic diagram of the non-tipping rod device. The rod can be treated as a rigid rod with its bottom end fixed at the hinge point O by the high strength thin wire and glue. Therefore, it can rotate around the hinge point O in the vertical plane. As shown in Fig. 1, The center of gravity of the hollow rod will be toward the bottom once a specific quantity of NaCl crystals has been introduced. Notice that the direction of gravity always acts vertically downward, while the direction of buoyancy always acts vertically upward. When the rod is subjected to horizontal wind, as shown in Fig.1, it

will induce a specific inclination angle, leading to the generation of gravitational torque ($\overrightarrow{M_G} = \vec{r_G} \times \vec{G}$), buoyant torque ($\overrightarrow{M_b} = \vec{r_b} \times \vec{F_b}$), wind torque ($\overrightarrow{M_w} = \vec{r_w} \times \vec{F_w}$) and water plane restoring torque ($\overrightarrow{M_{wp}}$).The four torques can achieve static moment equilibrium at the hinge point O, thereby ensuring the stability of the rod. As the wind speed increases, the angle of the rod will further increase, leading to a higher immersion ratio of the rod in the water. Hence, the buoyancy is enhanced, leading to a significant increase in the buoyant torque. Meanwhile, the wind force on the rod is mitigated by reducing the exposed area, resulting in increased stability of the rod.

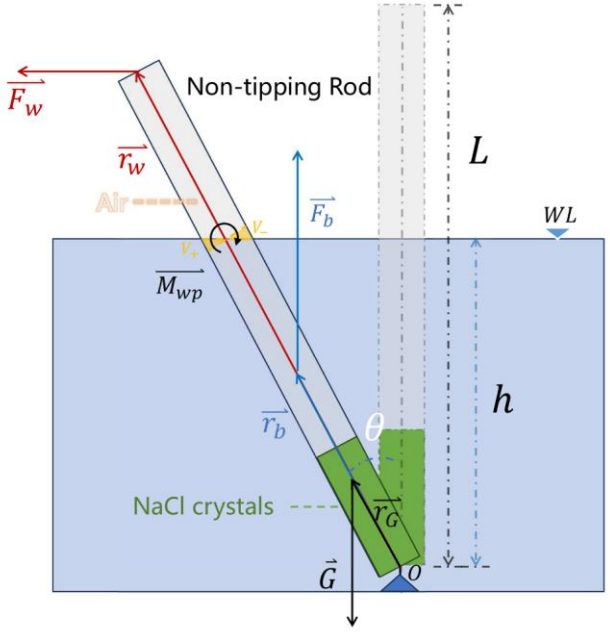

Fig.1. Schematic diagram of the non-tipping rod device.

2.3 Theoretical Analysis of Static Moment Equilibrium

Shown in Figure 1, the length of the rod is denoted as L, and the submerged length of the rod in a vertical position is denoted as h. When the rod is at an angle of θ, the buoyancy of the rod in water is $F_b = \rho g V = \rho g A h \sec\theta$, where A represents the rod cross section area and ρ represents the density of the water. Mathematically, the water plane restoring torque ($\overrightarrow{M_{wp}}$) is generated by the couple moment generated by both the positive buoyancy force of the submerged wedge (V_+) and the negative buoyancy force of the emerged wedge (V_-) [15-16],as illustrated in Fig. 1, and can be formulated as

$$M_{wp} = \rho g I_A \sin\theta (1 + \frac{1}{2}\tan^2\theta)$$

where $I_A = \frac{\pi D^4}{64}$ is the second moment of the rod's cross section area, in which D is the diameter of the rod. Analyzing the resultant torque on the rod, we define that its positive direction is perpendicular to the plane of the paper and point to it. Thus,

$$\begin{aligned}\overrightarrow{M} &= \overrightarrow{M_G} + \overrightarrow{M_b} + \overrightarrow{M_{wp}} + \overrightarrow{M_w} \\ &= \vec{r_G} \times \vec{G} + \vec{r_b} \times \vec{F_b} + \overrightarrow{M_{wp}} + \vec{r_w} \times \vec{F_w} \\ &= -\left|\vec{r_G}\right|\left|\vec{G}\right|\sin(\pi - \theta) + \left|\vec{r_b}\right|\left|\vec{F_b}\right|\sin\theta + \rho g I_A \sin\theta(1 + \frac{1}{2}\tan^2\theta) - \left|\vec{r_w}\right|\left|\vec{F_w}\right|\sin(\frac{\pi}{2} - \theta)\end{aligned}$$

When the rod is stabilized, the net torque acting on it becomes zero. The above formula can be simplified as follows.

$$\begin{aligned}0 &= -\left|\vec{r_G}\right|\left|\vec{G}\right|\sin\theta + \left|\vec{r_b}\right|\left|\vec{F_b}\right|\sin\theta + \rho g I_A \sin\theta(1 + \frac{1}{2}\tan^2\theta) - \left|\vec{r_w}\right|\left|\vec{F_w}\right|\cos\theta \\ &= -r_G G \sin\theta + \frac{h}{2\cos\theta}\rho g A \frac{h}{\cos\theta}\sin\theta + \rho g \frac{\pi D^4}{64}\sin\theta(1 + \frac{1}{2}\tan^2\theta) - L F_w \cos\theta\end{aligned}$$

Hence, the wind force F_w can be expressed as follows.

$$F_w = \frac{\rho g A h^2 \tan\theta \sec^2\theta}{2L} + \frac{\rho g \pi D^4 \tan\theta}{64L}(1+\frac{1}{2}\tan^2\theta) - \frac{r_G G \tan\theta}{L}$$

Let $a = \frac{\rho g A h^2}{2L}$, $b = \frac{\rho g \pi D^4}{64L}$, $c = \frac{r_G G}{L}$, we obtained,

$$F_w = a\tan\theta\sec^2\theta + b\tan\theta(1+\frac{1}{2}\tan^2\theta) - c\tan\theta \qquad (1)$$

Equation (1) represents the theoretical functional correlation between the horizontal wind force F_w and the inclination angle θ of the non-tipping rod device. The other measured parameters, $D = 43.00\ mm$, $L = 250.0\ mm$, $h = 125.0\ mm$, $r_G = 63.0\ mm$, $A = 1452.2\ mm^2$ and $G = 0.8878\ \mathrm{N}$, are substituted into the expressions for $a = \frac{\rho g A h^2}{2L}$, $b = \frac{\rho g \pi D^4}{64L}$, $c = \frac{r_G G}{L}$ while taking $g = 9.807\ \mathrm{m/s^2}$ and $\rho = 0.9972\times10^3\ \mathrm{kg/m^3}$. It can be derived that $a = 0.4438\ \mathrm{N}$, $b = 0.0066\ \mathrm{N}$ and $c = 0.2237\ \mathrm{N}$. Therefore, by substituting the values of a, b and c into equation (1),

$$F_w = 0.4438\tan\theta\sec^2\theta + 0.0066\tan\theta(1+\frac{1}{2}\tan^2\theta) - 0.2237\tan\theta \qquad (2)$$

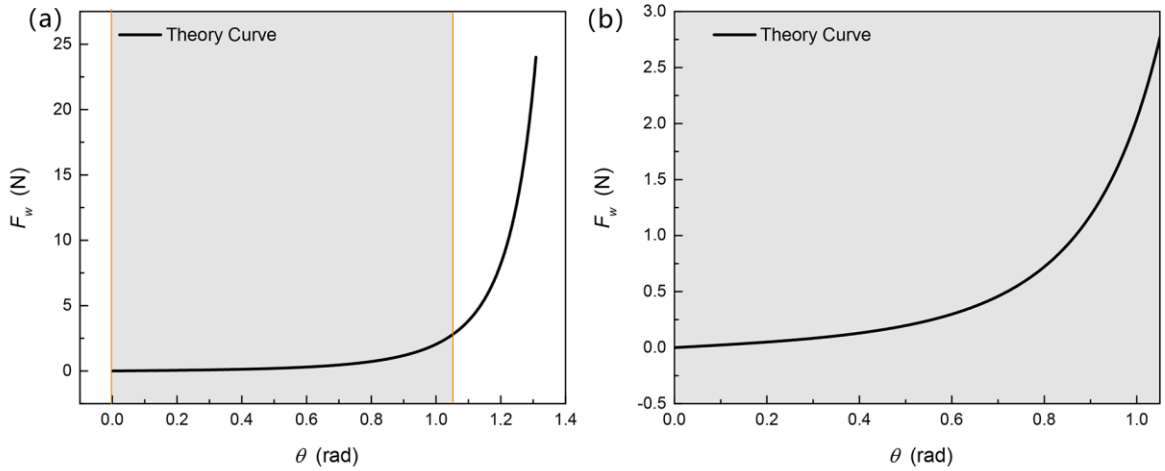

Fig. 2. (a) Theoretical curve of the horizontal wind force *versus* the inclination angle. (b) The enlargement figure of the gray area in (a).

The theoretical function image of F_w *versus* θ is shown in Fig. 2 (a). As depicted in the figure, the static moment equilibrium of the device exhibits half of a typical Pitchfork bifurcation diagram [17]. When considering the F_w in the opposite direction, it would form a complete Pitchfork bifurcation diagram. The gray area is the theoretical measurable area, the maximum inclination angle θ is up to 60 degrees (1.05 rad). Since the rod would be completely submerged in water without being affected by the wind while θ is more than 1.05 rad, which makes the rod device equipped with self-protection capabilities in super windy conditions. Figure 2(b) is an enlarged view of the gray area in Fig. 2(a). It can be seen from the Fig. 2(b) when the rod is initially in a vertical state, even a weak F_w can cause a noticeable θ. When the inclination angle θ exceeds 0.8 radians, the θ increases slowly with the rising.

A new physical quantity S (N/rad) is then defined to characterize the stability of the non-tipping rod at any given inclination angle θ. The value of S can be derived by taking the first derivative of function F_w with respect to variable θ, expressing as $S = \frac{dF_w}{d\theta}$. Hence,

$$S = a(1+2\sin^2\theta)\sec^4\theta + b(\frac{3}{2}\tan^2\theta+1)\sec^2\theta - c\sec^2\theta \qquad (3)$$

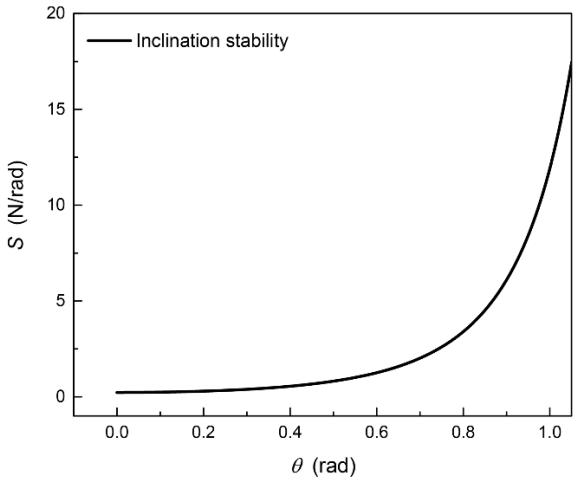

Fig. 3. Variation of theoretical stability with rod inclination angle.

The stability of the non-tipping rod S *versus* θ is shown in the above Fig. 3. It is evident that as the θ of the rod increases, so does the stability S, indicating a higher level of rod stability and increased wind force resistance, i.e., the sensitivity of the θ diminishes as F_w fluctuates. On the contrary, when the rod is vertical or less than 0.6 radians, even a slight wind disturbance will result in a significant increase in rod inclination, as confirmed by the subsequent experiments.

2.4 Device Preparation

1)The hollow plastic rod, sealing ring, and sealing cover were designed by the Bombo STEAM programmed robot ET841 and made by a plastics company.

2)Using a vernier caliper to measure the length *L*=250.0±0.08 mm (P=0.68) and the diameter *D*=43.0±0.02 mm (P=0.68) of the rod. See Supplemental material part 1 for calculation and analysis of measurements uncertainty.

3)Seal the bottom of the plastic hollow rod with a sealing cover by a glue gun and fix a high strength short thin wire in the center of the bottom. Then, wrap raw material belt around the bottom sealing ring for secondary sealing to enhance the sealing effectiveness.

4)Place a thin layer of NaCl crystals in the rod, followed by positioning a 3-axis wireless inclinometer sensor horizontally as shown in the Fig. 4(a). The wireless sensor is connected to the computer via Bluetooth and is capable of real-time recording of current 3D angle information, as depicted in Fig. 4(b). Then, add an appropriate amount of NaCl crystals to fully cover the sensor and use a sealing ring to compact the crystals, ensuring a horizontal solid layer. Record the thickness of the solid layer for consistency in future experiments, and finally cover the top of the rod with another sealing ring with a thin wire in the center.

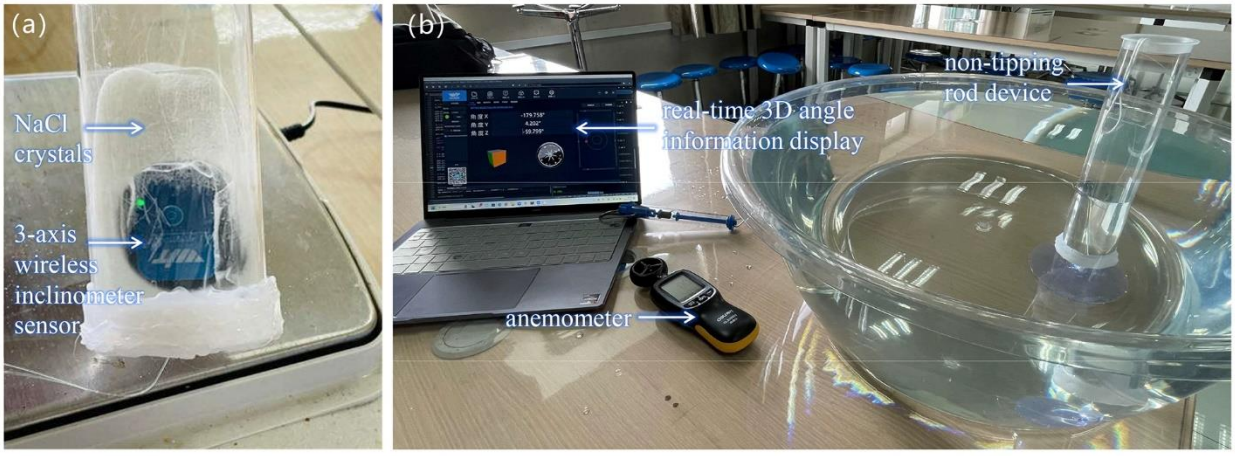

Fig. 4. (a) The interior diagram of the rod. (b)The computer displays real-time 3D angle information from the sensor.

5)Using a high precision electronic balance to weigh the mass of the entire rod *m*=90.53±0.02 g (P=0.68).

6)The center of gravity position of the entire rod is determined by using the suspension method with only a rubber band, thus measuring r_G=63.00±0.08 mm (P=0.68). The NaCl-air ratio in the rod allows for handy adjustment of the center of gravity.

7)Hang the short thin wire from the bottom of the rod onto the chuck attached to the base of large sink. Make sure that the wire is as short as possible to ensure that the hinge point O of the rod remains basically unchanged.

8)Start adding water to the large sink until the rod can stand vertically, then add a 1-2 cm layer of water to enhance stability. Hence, the buoyancy center can be conveniently adjusted by the sinking degree of the rod in the water. Gently push the rod, it should quickly return to its vertical position.

2.5 Experimental Procedures

1)The length of the rod immersed in water is measured to be *h*=125.0±0.1 mm (P=0.68) , the distance between the center of buoyancy and the hinge point O can be calculated as $r_b = \frac{h}{2\cos\theta}$,as depicted in Fig. 1.

2)After stabilizing the rod vertically, a spring dynamometer with an accuracy of 0.02 N is attached to the thin wire at the top. The rod is then pulled horizontally to record the sensor's inclination data θ under different tension force until it is almost completely submerged in water. The tension force here is designed equivalent to the horizontal wind force F_w. The experiment was repeated 3 times to minimize measurement error and enhance data accuracy. The experiment data are shown in Table 1. in RESULTS AND DISCUSSION part.

3)The flat outlet blower is utilized for ensuring maximum horizontal wind output, and different wind speed are recorded by an anemometer at various distances.

4)When the blower is aligned with the top of the rod, the equivalent horizontal wind force F_w is at the top of the bar, so it can be approximated that $r_w = L$ in Fig. 1. Based on the data recorded in the previous step, it is sufficient to measure the distance between the outlet and the top of the rod in order to determine the wind speed. The sensor is capable of real-time recording the inclination angle θ, thus enabling the acquisition of experimental data on the relationship between wind speed and θ.

5)Analyze the data between F_w and inclination angle θ in the step 2) to revise equation (1), explore the relationship between wind speed and θ for further analyzing the functional relationship between wind speed and F_w on the rod. More information of experimental conditions and precautions can be found in Supplemental material part 2.

3. RESULTS AND DISCUSSION

The data obtained by step 2) of 2.5 are as follows:

Table 1. Corresponding data of horizontal tension force and inclination angle

F_w (N)	0	0.04	0.06	0.08	0.10	0.12	0.16	0.20	0.24	0.28	0.32	0.38
θ_1 (rad)	0.00	0.39	0.42	0.46	0.48	0.50	0.54	0.58	0.61	0.63	0.66	0.69
θ_2 (rad)	0.00	0.33	0.40	0.43	0.45	0.49	0.53	0.57	0.60	0.63	0.64	0.67
θ_3 (rad)	0.00	0.32	0.38	0.43	0.45	0.49	0.54	0.57	0.60	0.63	0.65	0.68
$\overline{\theta}$ (rad)	0	0.35	0.4	0.44	0.46	0.49	0.54	0.57	0.61	0.63	0.65	0.68
F_w (N)	0.44	0.50	0.56	0.62	0.72	0.82	0.92	1.02	1.32	1.52	1.72	2.02
θ_1 (rad)	0.71	0.73	0.75	0.77	0.79	0.82	0.85	0.87	0.88	0.90	0.91	0.93
θ_2 (rad)	0.69	0.73	0.74	0.76	0.78	0.80	0.83	0.85	0.88	0.91	0.92	0.93
θ_3 (rad)	0.70	0.72	0.74	0.76	0.78	0.81	0.83	0.84	0.89	0.91	0.93	0.93
$\overline{\theta}$ (rad)	0.70	0.73	0.74	0.76	0.78	0.81	0.83	0.85	0.88	0.90	0.92	0.93

Table I. gives the experimental data of horizontal wind force F_w and the rod inclination θ. All data are deducted from background errors. The $\overline{\theta}$ in the chart represents the mean value of three measurements of θ to minimize measurement error. The data of $\overline{\theta}$ were plotted in the Fig. 5 as red solid points. Based on the obtained theoretical equation (2), actual measurements and other potential factors may result in certain variations in the values of a and c .The magnitude of b is approximately two orders of magnitude smaller than that of a and c, thus the impact of changes in b can be disregarded. Therefore, two parameters A and C can be introduced for fitting adjustments to the values a and c. Therefore, the equation

$$F_w = (0.4438 + A)\tan\theta\sec^2\theta + 0.0066\tan\theta(1+\frac{1}{2}\tan^2\theta) - (0.2237 + C)\tan\theta$$

was utilized to fit the experimental data points in the Fig. 5. The Levenberg-Marquardt algorithm was employed to obtain the fitting results, as depicted by the red fitting curve in the Fig. 5. The red curve represents the actual experimental function of F_w and θ.

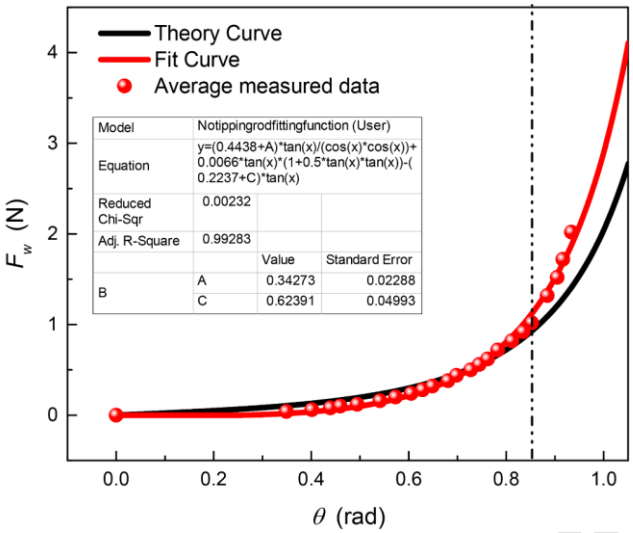

Fig. 5. The actual relationship between the horizontal wind force and the rod inclination angle.

It can be seen from the Fig. 5 that the data can perform very good fitting. The Adjusted R-Square is 0.99283, indicating that the function model has high accuracy. From the Fig.5, the red curve indicates that the maximum F_w value can reach the upper limit of 4.11 N with uncertainty of ±0.04 N (P=0.95) according to analysis of synthetic uncertainty in the Supplemental material part 1. The values of A and C in the fitting function, as shown in the table of the figure, are determined to be 0.3427 and 0.6239 respectively. Therefore, it can be concluded that the actual experimental function image satisfies the following equation (4).

$$F_w = 0.7865\tan\theta\sec^2\theta + 0.0066\tan\theta(1+\frac{1}{2}\tan^2\theta) - 0.8476\tan\theta \qquad (4)$$

To ensure the validity of the experiment and the reliability of equation (4), a double-blind verification was carried out. After applying a force of 1 N, the experiment yielded an inclination measurement of 47.80 degrees, while the calculation from equation (4) resulted in an inclination of 0.83 radians (47.73 degrees), demonstrating the high reliability of the equation.

Simultaneously, for the purpose of contrasting the disparity between the experimentally fitted curve and the theoretically calculated curve, both are plotted in Fig. 5 for intuitive comparison. As depicted in the figure, for θ less than 0.85 radians, the discrepancy between the two curves is negligible. However, for θ exceeding 0.85 radians, the experimental F_w surpasses the theoretical calculation value. The primary factor for this phenomenon is that when the θ exceeds 0.85 radians, the hinge point O ceases to remain stationary and undergoes a slight displacement. This slight displacement will cause the rod to experience a counteracting force opposite to the direction of the F_w, resulting in a greater F_w than the theoretical value at the same inclination. The revised values of A and C are large due to the same reason.

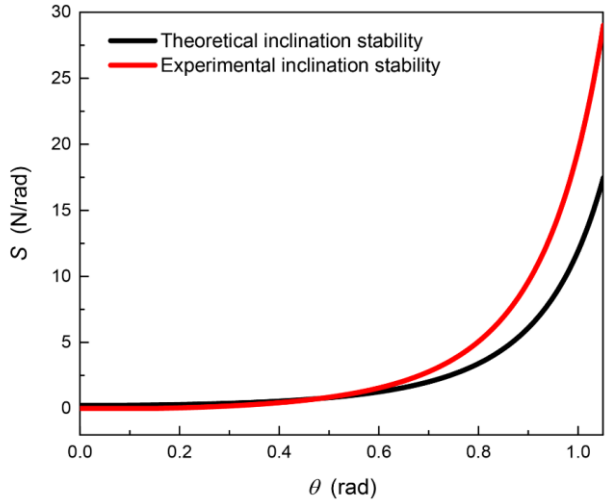

Fig. 6. Theoretical and experimental inclination stability curves.

Furthermore, when comparing the stability of the two at any given inclination angle as depicted in Fig. 6, it is evident that the actual rod exhibits a higher level of stability.

The relationship between wind speed and inclination angle is then studied according to steps 4) and 5) of section 2.5. It is discovered that when horizontal wind encounters the rod, end streams will be generated, and water surface wave disturbance will be caused by the wind. This results in a significant lack of stability of the rod, posing great difficulties for studying the relationship between wind speed and inclination angle. This process also needs additional simulation analysis of fluid mechanics and aerodynamics [9, 17-18], which is not further elaborated here. As a result, this paper provides a qualitative conclusion that the device can withstand at least the wind of near gale [19]. Since when the wind speed is 16.3 m/s, the rod inclination is only 0.51 radians, as analyzed in Supplemental material part 3.

4. CONCLUSION

In this paper, a simple and practical non-tipping rod device is constructed based on the principle of static moment equilibrium. The device can maintain balance in water without being overturned by an external wind torque. The rod allows for handy adjustment of the center of gravity and the buoyancy center, with the inclination angle recorded by the three-axis sensor in the rod. The angle of the vertical rod θ will increase with the horizontal wind force F_w, and as the θ increases, the rod exhibits greater stability. This result is supported by both theoretical analysis and experimental data. Meanwhile, the precise functional relationship equation (4) is derived by the theoretical analysis and modified by the experimental data, which is confirmed by the double-blind verification. The device is capable of detecting wind force up to 4.11±0.04 N and can withstand at least the wind of near gale. This intuitive experimental device can be used as a demonstration experiment for teachers to expound the idea of static moment equilibrium and it has potential applications in the fields of wind detection engineering.

REFERENCES

1. David Halliday, Robert Resnick, Jearl Walker. Fundamentals of physics. John Wiley & Sons; 2013.
2. Michael E Plesha, Gary L Gray, Francesco Costanzo. Engineering Mechanics: Statics. McGraw-Hill Higher Education New York, NY, USA; 2010.
3. A Luévanos Rojas. Method of structural analysis for statically indeterminate beams, International Journal of Innovative Computing. Information and Control. 2012;8(8):5473-5486.
4. Mohammad Jafari, Partha P Sarkar. Wind-induced response characteristics of a yawed and inclined cable in ABL wind: Experimental-and numerical-model based study. Engineering Structures. 2020; 214:110681.
5. Henry L Langhaar. Energy methods in applied mechanics. Courier Dover Publications; 2016.
6. Davide Bigoni. Extremely Deformable Structures. Springer Vienna, Vienna; 2015.
7. Terrence Toepker, Archimedes Revisited and Beyond, The Physics Teacher. 2023;61(9): 780-784.
8. Y. Z. Liu, J. W. Zu. Stability and bifurcation of helical equilibrium of a thin elastic rod. Acta Mechanica. 2004;167(1): 29-39.
9. Varghese Mathai, Laura AWM Loeffen, Timothy TK Chan, Sander Wildeman. Dynamics of heavy and buoyant underwater pendulums. Journal of Fluid Mechanics. 2019; 862:348-363.
10. Timothy Bretl, Zoe McCarthy. Quasi-static manipulation of a Kirchhoff elastic rod based on a geometric analysis of equilibrium configurations. The International Journal of Robotics Research. 2014;33(1):48-68.
11. Prashant K. Purohit. Plectoneme formation in twisted fluctuating rods. Journal of the Mechanics and Physics of Solids. 2008;56(5):1715-1729.
12. W. B. Fraser, D. M. Stump. The equilibrium of the convergence point in two-strand yarn plying. International Journal of Solids and Structures. 1998;35(3):285-298.
13. C. L. Lu, N. C. Perkins. Complex spatial equilibria of u-joint supported cables under torque, thrust and self-weight. International Journal of Non-Linear Mechanics. 1995;30 (3): 271-285.
14. Sangrok Jin, Jihoon Kim, Jangho Bae, TaeWon Seo, Jongwon Kim, Design. modeling and optimization of an underwater manipulator with four-bar mechanism and compliant linkage. Journal of Mechanical Science and Technology. 2016;30(9):4337-4343.
15. Mohammed Khair Al-Solihat, Meyer Nahon. Nonlinear hydrostatic restoring of floating platforms. Journal of Computational and Nonlinear Dynamics. 2015;10(4):041005.
16. Adrian Biran, Rubén López-Pulido. Ship hydrostatics and stability. Butterworth-Heinemann; 2013.

17. Mohammed Khair Al-Solihat. Nonlinear static and dynamic behaviors of partially and fully submerged rod pendulums in quiescent water. Nonlinear Dynamics; 2024.
18. Dominik Worf, Ali Khosronejad, Thomas Gold, Kevin Reiterer, Helmut Habersack, Christine Sindelar. Fluid structure interaction of a subaqueous pendulum: Analyzing the effect of wake correction via large eddy simulations. Physics of Fluids. 2022;34 (5).
19. Dennis Wheeler, Clive Wilkinson. FROM CALM TO STORM: THE ORIGINS OF THE BEAUFORT WIND SCALE. The Mariner's Mirror. 2004;90(2):187-201.